Catalysis Today 422 (2023) 114214

Contents lists available at ScienceDirect

Catalysis Today

journal homepage: www.elsevier.com/locate/cattod

Laser-induced tuning of carbon nanosensitizers to maximize nitrogen doping and reactive oxygen species production in the visible range

Ainhoa Madrid [a,b,c], Gema Martinez [a,b,c,1], Felipe Hornos [a,b,1], Javier Bonet-Aleta [a,b,1], Esteban Calvo [d], Antonio Lozano [e], Jose L. Hueso [a,b,c,f,*]

[a] Instituto de Nanociencia y Materiales de Aragón (INMA), CSIC-Universidad de Zaragoza, Campus Rio Ebro, Edificio I+D, C/ Poeta Mariano Esquillor, s/n, 50018 Zaragoza, Spain
[b] Department of Chemical and Environmental Engineering, University of Zaragoza, Campus Rio Ebro, C/María de Luna, 3, 50018 Zaragoza, Spain
[c] Networking Research Center in Biomaterials, Bioengineering and Nanomedicine (CIBER-BBN), Instituto de Salud Carlos III, 28029 Madrid, Spain
[d] Departamento de Mecánica de Fluidos, Escuela de Ingeniería y Arquitectura, Universidad de Zaragoza, C/ María de Luna, 3, 50018 Zaragoza, Spain
[e] Instituto de Carboquímica (ICB-CSIC), Campus Río Ebro, C/ María de Luna, 3, 50018 Zaragoza, Spain
[f] Instituto de Investigación Sanitaria (IIS) de Aragón, Avenida San Juan Bosco, 13, 50009 Zaragoza, Spain

ARTICLE INFO

Keywords:
Carbon Dots
Nitrogen doping
Laser Pyrolysis
P25
Photocatalysis
ROS

ABSTRACT

Carbon nanodots (CNDs) have emerged as novel fluorescent nanosensitizers able to expand the photocatalytic response of conventional semiconductors beyond the ultraviolet spectral window. Key aspects of CNDs related with their high photostability, resistance to photobleaching and optical properties (including downconversion and upconversion luminescence) are often associated with the capacity to dope the carbogenic network with light heteroatoms, especially nitrogen. In this work, we present the use of laser pyrolysis as a versatile and convenient synthesis technique to generate different N-doped CNDs. The level of N doping can be tuned through the selection of a single liquid solvent containing N as carbon precursor. This liquid precursor can be alternatively enriched with additional N sources co-fed in the form of gas (i.e. NH_3) or disolved solid precursors (i.e. phtalocyanine-Ph). We demonstrate that the N-CNDs retrieved after the additional N cofeeding treatments improve their photoactivity when assembled to P25 nanoparticles towards the conversion of methyl orange (MO) under white LED illumination. All the N-CNDs act as photosensitizers expanding the response of P25 beyond the UV region and exhibit an active role generating different types of Reactive Oxygen Species (ROS) via singlet oxygen, superoxide and hydroxyl radicals that can pave the way for multiple potential applications in environmental and green processes.

1. Introduction

Nanostructured photocatalysts represent one of the greener approaches that takes advantage of natural or artificial light to generate electron-hole pairs able to induce chemical reactions to degrade (or upgrade) organic molecules via redox processes induced by reactive oxygen species (ROS) [1,2]. The major drawbacks are related with the limited number of photoactive materials effectively working beyond the UV region. This means that around 94 % of the solar spectrum is not fully exploited. In the past years, there has been an intense research in the field to find new photocatalysts able to expand their photo-response towards the visible-near infrared (vis-NIR) window [2–7]. The most successful approaches involve the formation of heterogeneous structures or the addition of co-catalysts, mostly noble or transition metals. These structures are able to delay the electron-hole recombination rates of regular photocatalysts, thereby increasing their reactivity. Organic molecules have been also exploited as sensitizers or light harvesters able to generate ROS by direct energy transfer (for instance to form the highly reactive singlet oxygen species) [1,3,8–11].

Carbon nanodots (CNDs) have emerged in the past 15 years as novel fluorescent nanosensitizers [2,8,10–13] that combine a series of appealing properties such as: (i) high colloidal stability in amphiphilic media; (ii) high photo-stability and resistance to photobleaching; (iii) reduced toxicity in comparison with nanosystems containing heavy

* Corresponding author at: Instituto de Nanociencia y Materiales de Aragón (INMA); CSIC-Universidad de Zaragoza, Campus Rio Ebro, Edificio I+D, C/ Poeta Mariano Esquillor, s/n, 50018, Zaragoza, Spain.
E-mail address: jlhueso@unizar.es (J.L. Hueso).
[1] These authors contributed equally.

https://doi.org/10.1016/j.cattod.2023.114214
Received 30 November 2022; Received in revised form 4 May 2023; Accepted 17 May 2023
Available online 18 May 2023

metal and potentially toxic elements; (iv) tunable optical response spanning from UV to NIR ranges including large two-photon excitation cross-sections; (v) abundance of inexpensive raw precursors for their synthesis. Carbon dots have proven themselves as excellent alternatives to organic molecules able to expand the photocatalytic response of other semiconductors as decorating photosensitizers. Their photoluminescence make them suitable for diagnostic, delivery and phototherapy application in the biomedical field, sensing, photoreforming of wastes or visible-NIR enhanced photodegradation of organic pollutants [2,4,8,10,11,13,14–24]. Remarkably, the photocatalytic role of CNDs is based on their optical response as nanostructured semiconductors and their capability to form electron-hole pairs upon irradiation with light. Furthermore, these charge carriers can induce the generation of different ROS depending on the nature of the CNDs [1,6,24].

In contrast to other synthesis approaches, the exquisite control of the feeding precursor can make laser pyrolysis an excellent technique to tailor composition and properties to yield a wide plethora of nanomaterials including CNDs [25–31]. In a recent work, Mas et al. [4] demonstrated the accuracy and control of laser pyrolysis to produce CNDs. They showed how a simple modification in the stoichiometry of the feeding solvents (toluene vs. pyridine) led to different outcomes in terms of optical properties and photocatalytic response of the fabricated CNDs. Herein, we describe the use of laser-driven pyrolysis of organic precursors as a suitable methodology to develop multifunctional CNDs with extended N doping levels. Using the laser-driven decomposition of pyridine as starting point, additional N-doping is achieved upon co-feeding additional N sources either in gas (e.g. ammonia) and/or suspended solids (e.g. macrocycles such as phtalocyanines). The assembly of these CNDs with P25 NPs enhances the visible-light driven decoloration of methyl orange (MO) using white emitting LEDs. Interestingly, the CNDs act as photosensitizers able to generate singlet oxygen ($^1O_2$), hydroxyl ($^{\bullet}OH$) and superoxide ($^{\bullet}O_2^-$) as the main ROS contributing species [32] with a preferential contribution depending on the type of predominant surface chemical groups.

2. Experimental section

2.1. Nitrogen-doped carbon nanodots by laser pyrolysis

The synthesis of the CNDs was carried out by laser pyrolysis of different N-containing precursors fed through different approaches (Fig. 1). The first step was the optimization of the process parameters.

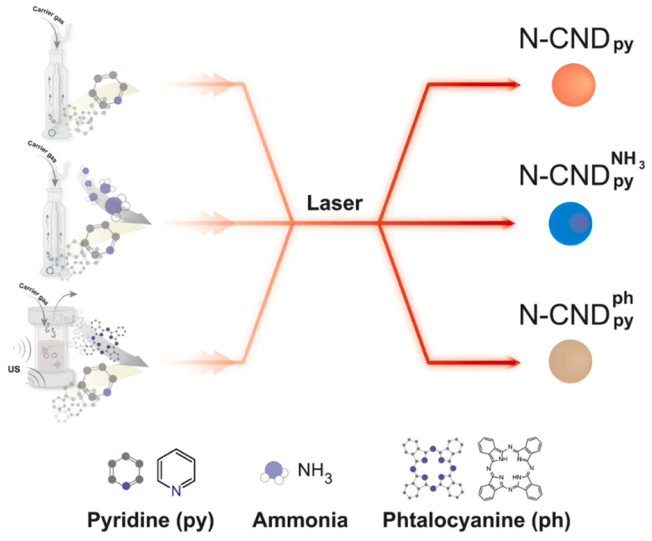

Fig. 1. Simplified scheme of the synthesis of different N-doped CNDs using laser pyrolysis (cw CO_2 infrared laser) and feeding different N-containing precursors.

These include precursor concentration, gas flow rates, pressure and laser power [26,33]. The optimized reaction conditions used in this work are listed in Table 1. Pyridine was selected as the main liquid solvent to be fed into the reaction chamber from a sealed vessel equipped with regulatory opening-close valves. 30 sccm of sulfur hexafluoride (SF_6) were fed to sensitize the infrared laser and 130 sccm of argon (Ar) was used as carrier gas passing through the organic precursor reservoir. A second set of experimental conditions was set in order to increase the N percentage in the CNDs. In this case, besides pyridine, a feeding flow of ammonia (NH_3) was co-fed with the Ar and the sensitizer (see Table 1). Finally, a third strategy to increase the N doping level consisted on the redispersion of a solid macrocycle like phtalocyanine (ph) in pyridine (Fig. 1) (total of 25 mL of pyridine containing 8.3 mM of ph). In this latter case, the solution was fed from a sealed chamber equipped with a 1.65 MHz nebulizer, working at 40 V. A set of regulatory opening-close valves allowed the purge of the chamber, as well as the transit of the carrier gas.

A CO_2 laser ($\lambda = 10.6$ μm) was placed to interact with the reactant streams in a 90 º configuration. A laser power of 275 W was required for the active decomposition of precursors. The as-prepared nanoparticles were directly collected in a liquid trap containing triethylenglycol (TREG). The laser experiments were settled for 6 h. The resulting suspensions were labeled as N-CND_{py}, N-CND_{py}^{NH3} and N-CND_{py}^{ph} depending on the precursor and the co-feeding agent used for their synthesis. The resulting suspensions containing the carbon dots were centrifuged and washed with ethanol to remove TREG excess (15 ºC, 15,000 rpm, 30 min). The assembly of the N-CNDs onto P25 NPs was carried out following a protocol described elsewhere [4]. The synthesis of these materials were performed at the Synthesis of Nanoparticles Unit (UNIT 9) of the ICTS "NANBIOSIS" at the Institute of Nanoscience and Materials of Aragon (INMA)-Universidad de Zaragoza.

2.2. Photocatalytic tests under white LED irradiation

Methyl orange (MO) degradation reactions were performed under air inside fluorescence quartz cuvettes (1 cm light path) containing 4 mL of aqueous MO solution (40 μM), 1 mM H_2O_2 in formic buffer (50 mM) at pH 4 or HEPES buffer at pH 7 (50 mM) and different catalyst concentrations of 0.1 mg/mL. Irradiations were carried out, with continuous stirring, using a cylindrical reactor (equipped with LED lamps, emission output 400–700 nm, 392.7 mW/cm^2) placed 1 cm from the cuvette. At certain time intervals, an aliquot of the volume was removed and filtered through a 0.22 μm filter to remove the catalyst. The evolution was monitored up to 2 h and the spectra were acquired in a spectrophotometer (Shimadzu) from 300 to 600 nm. Photolysis experiments were carried out using MO in the absence of the catalyst, under the same conditions of H_2O_2 concentration and buffer.

2.3. Identification of reactive oxygen species

The identification of singlet oxygen species was performed using fluorescence quartz cuvettes (1 cm light path) containing 4 mL of aqueous solution of the singlet oxygen probe 9,10-Anthracenediyl-bis

Table 1
Summary of experimental conditions for the laser pyrolysis reactor.

Feeding rates (mL/min)	**Without NH_3**	**With NH_3**
	SF_6: 30 Ar: 130	SF_6: 30 Ar: 80 NH_3: 50
Carrier and focus gas flow rates (mL/min)	Ar (coaxial): 110 N_2 (window): 200 Ar (window): 600	
Laser power (W)	275	
Working pressure (mbar)	150	

Pyridine was supplied pure or containing a 8.3 mM concentration of dissolved phtalocyanine.

(methylene)dimalonic acid (ABDA) [34–37] (10 μM), 1 mM of H_2O_2 in formic buffer (50 mM) at pH 4 and different catalyst at 0.1 mg/mL. Irradiations were carried out, with continuous stirring, using a cylindrical reactor (equipped with LED lamps, 400–700 nm emission output, 392.7 mW/cm^2) placed 1 cm away from the cuvette. At certain time intervals, an aliquot of the volume was removed and filtered through a 0.22 μm filter to remove the catalyst. Prior to measurement, 100 μL of filtered solution was diluted in 3000 μL of water and measured on a LS 55 fluorescence spectrometer (PerkinElmer). λ_{exc}/ λ_{em} = 375 nm/400–500 nm, slit-widths of 2.5 nm for both excitation and emission wavelengths. The evolution was monitored over time 10 min. Control experiments were performed by using ABDA in the absence of the catalyst. Experiments in the absence of O_2 were also performed following the same protocol after purging the suspensions with an Ar flow for 15 min.

The identification of hydroxyl radicals was performed using fluorescence quartz cuvettes (1 cm light path) containing 2 mL of aqueous solution of the hydroxyl probe sodium terephthalate [19,22,38] (NaTA) (2.5 mM), 1 mM of H_2O_2 in formic buffer (50 mM) at pH 4 and different catalyst at 0.1 mg/mL. Irradiations were carried out, with continuous stirring, using a cylindrical reactor (equipped with LED lamps, 400–700 nm emission output, 71.7 mW/cm^2) placed 1 cm away from

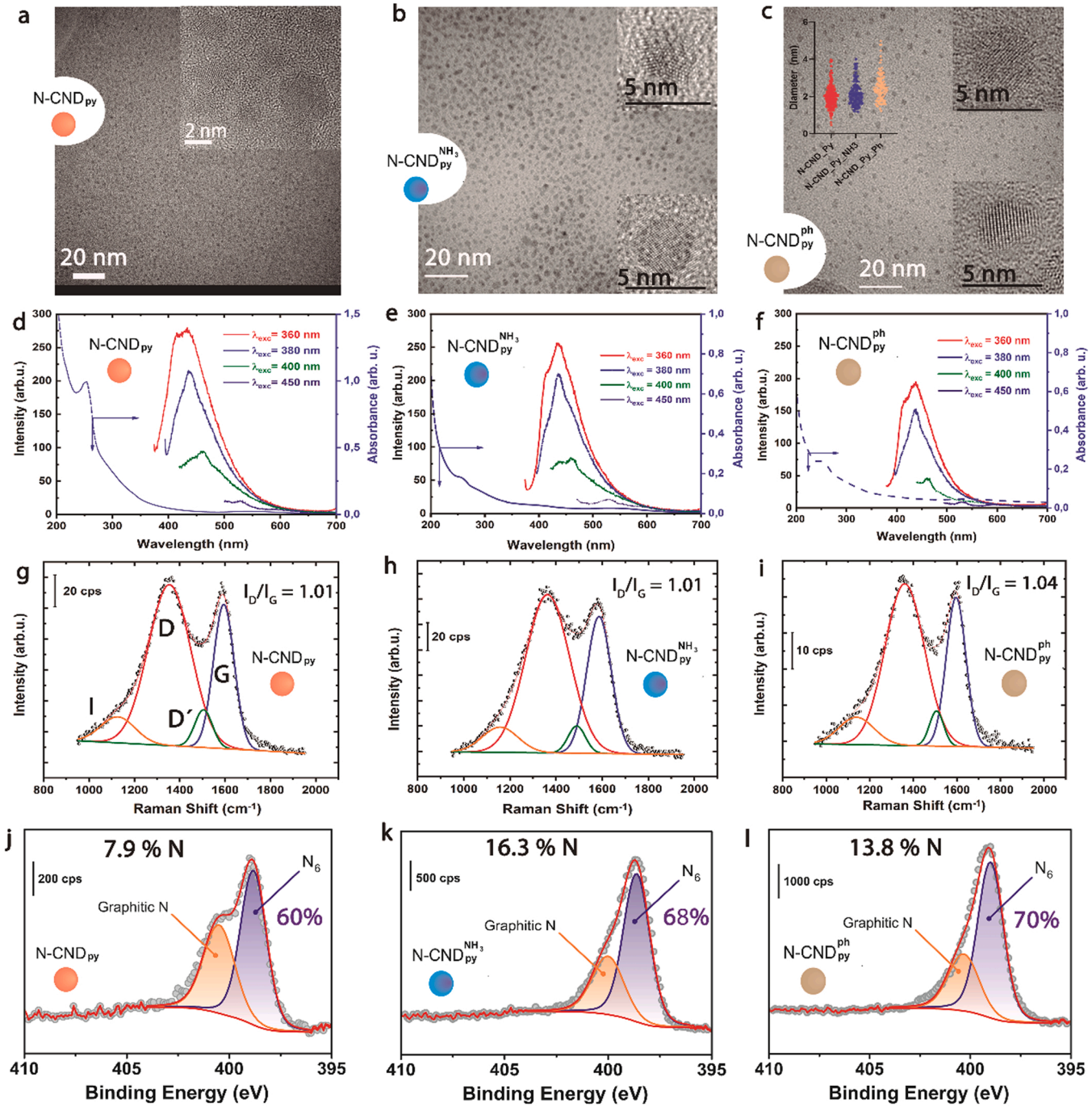

Fig. 2. Characterization of the N-CNDs synthesized by laser pyrolysis: a)-c) TEM and HRTEM images corresponding to the different CNDs obtained by pyrolysis of pyridine, pyridine + ammonia and pyridine + phtalocyanine, respectively; d)-f) Absorption spectra (blue line) and photoluminescence (PL) spectra for a range of excitation wavelengths (360–450 nm); g)-i) Raman Spectra corresponding to the CNDs generated by laser pyrolysis, including fitting analysis and I_D/I_G ratios; j)-l) X-ray photoemission spectra corresponding to the N1s region, including N at. % and fittings.

the cuvette. After 10 min, the solution was filtered through a 0.22 μm filter to remove the catalyst and measured on a LS 55 fluorescence spectrometer (PerkinElmer). $\lambda_{exc}/\ \lambda_{em}$ = 315 nm/330–550 nm, slit-widths of 7.5 nm for both excitation and emission wavelengths. Control experiments were performed by using NaTA in the absence of the catalyst.

The identification of superoxide radical species was performed using fluorescence quartz cuvettes (1 cm light path) containing 2 mL of aqueous solution of the superoxide probe dihydroethidium [20,39,40] (DHE) (50 μM), 1 mM of H_2O_2 in formic buffer (50 mM) at pH 4 and different catalyst at 0.1 mg/mL (It was also repeated without H_2O_2). Irradiations were carried out with continuous stirring, using a cylindrical reactor (equipped with LED lamps, 400–700 nm emission output, 71.7 mW/cm^2) placed 1 cm away from the cuvette. After 10 min, the solution was filtered through a 0.22 μm filter to remove the catalyst and measured on a LS 55 fluorescence spectrometer (PerkinElmer). $\lambda_{exc}/\ \lambda_{em}$ = 480 nm/500–700 nm, slit-widths of 10 nm for both excitation and emission wavelengths. Control experiments were performed by using DHE in the absence of the catalyst. A control experiment in the absence of LED was also performed with no evidence of activity (data not shown).

3. Results and discussion

3.1. Synthesis and characterization of N-doped carbon nanodots retrieved by laser pyrolysis: effect of co-feeding a second nitrogen precursor

The laser-driven pyrolysis of pyridine in the absence and presence of NH_3 (CND_{py} and N-CND_{py}^{NH3}, respectively) rendered N-CNDs with similar diameter size distributions around 1.9 nm (Fig. 2a-b and inset 2c). The sample nebulized containing phtalocyanine N-CND_{py}^{ph}) yielded slightly higher mean diameters closed to 2.3 nm and a wider dispersion (Fig. 2c). HR-TEM images confirmed the crystalline graphitic nature of the CNDs (insets in Fig. 2a-c) expected from the highly energetic reaction conditions occurring in the intersection spot of the precursors and the CO_2 laser. The absorption spectra of all the CNDs showed the typical π-π * transition band at 250–275 nm with a decreasing intensity from CND_{py} to N-CND_{py}^{NH3} and N-CND_{py}^{ph} (Fig. 2d-f) [7,13]. Likewise, the absorption contribution at 340–350 nm associated to n-π * transitions of the N sites also seemed to diminish with respect to the CND_{py}. The absorption spectra broadly expanded towards the visible range as previously reported for other N-enriched CNDs. All the CNDs exhibited a wavelength-independent photoluminescence (PL) emission range with λ_{em} centered at 450 nm and λ_{exc} = 360–400 nm (Fig. 2d-f). These optical behavior suggest a narrow size distribution and composition of CNDs emitters where the graphitic order is being disrupted by the presence of N, thereby leading to a new electronic configuration where the radiative decay of excited electron proceeds from N energy states [4,7,13,41].

Fig. 2g-i show the Raman spectra corresponding to the three N-CNDs. All the spectra were fitted according to previous reports available in the literature [42–44]. The major contributions were centered at ~1354 cm^{-1} and ~1594 cm^{-1}. The former is typically denoted as D band and correspond to the presence of local distortions and disordered graphitic planes. The latter correspond to the G band and accounts for the vibrational mode of ordered graphitic crystal planes with sp^2 bonds. Secondary contributions typically labelled as D´and I and identified at ~1500 and ~1200 cm^{-1} are also indicative of local disorder. The three samples showed an analogous distribution of all the fitting components but addressing the calculation of the I_D/I_G ratio, there was an increase from 1.01 to 1.04 in the N-CND_{py}^{ph} sample. Therefore, the ratio of disordered carbon structure (i.e. sp^3 to sp^2 ratio) seems to be higher in the carbon dots processed with the macrocycle co-feeding (Fig. 2g to i).

The analysis of the surface composition further confirmed the presence of N-C bonds and the N-enrichment in the samples retrieved from the two co-feeding experiments. A two-fold increase of atomic N % was determined (Fig. 2j-l and Table S1). The N1s region was fitted with two main contributions at 399.4 eV and 401–402 eV, respectively. The first contribution at 399.4 eV was attributed to N in terminal or bridged positions [45,46]. The second contribution was assigned to graphitic N quaternary amines [45,47,48]. Interestingly, the co-feeding with NH_3 or phtalocyanine progressively reduced the contribution of these graphitic N [46] (Fig. 2j-l). It is also worth mentioning that the analysis of other regions revealed: i) an increasing contribution of C-O/C-N species at 285.7 eV (Fig. S1a-S1c); ii) a reduction of the presence of oxygen in the O1s region (Table S1), especially O-Csp3 bonds (Fig. S1d-S1f) and iii) an enrichment of S % (Fig. S1g-S1i and Table S1). The characterization of the different N-CNDs corroborates the success of both co-feeding strategies to increase the N-doping levels. In comparison with the original condition using only pyridine as precursor, the other experimental conditions led to a progressive reduction of the graphitic order, a reduction in the number of oxygen defects and a surface enrichment with N terminal groups. As a result, a preferential wavelength-independent PL emission was detected in contrast to the wavelength dependent PL emission displayed by more oxygenated CNDs [7].

3.2. Photocatalytic activity of the assembled N-doped carbon dots under white LED illumination

Based on previous reports available in our group and in the literature, the N-CNDs were tested as potential photosensitizers of P25 NPs to expand their response beyond the UV region [2,11,24]. As described in the experimental section, the N-CNDs were collected and attached to P25 NPs via impregnation followed by drying under vacuum (Fig. 3a). TEM and HAADF-STEM analysis of the different composites acknowledged the homogeneous distribution of the N-CNDs onto the semiconductor support (Fig. 3b-d). Moreover, an expanded absorption spectrum towards the visible to NIR range was observed in comparison with the uncoated commercial P25 NPs (Fig. 4a). This is attributable to the contribution of extra n-π * transitions provided by N energy surface states that will contribute to narrow the band gap of the hybrid material [49,50].

The visible-light driven photodegradation of methyl orange (MO) was evaluated in the absence of photocatalysts and in the presence of uncoated P25 NPs and the different N-CNDs@P25 hybrids. The organic model dye was subjected to illumination with a high intensity white LED (see experimental section for details) and feeding H_2O_2 as oxidant agent. The experiments were carried out at two different fixed pH conditions using buffers (pH=4 and pH=7). The experiments at higher pH yielded a maximum MO degradation of 20 % for the N-CND@P25 hybrids after 2 h irradiation, only slightly higher than the uncoated P25 NPs (Fig. 4b). In contrast, the experiments carried out at lower pH showed different and significant degradation trends for the composites containing the N-enriched CNDs (Figs. 4c and S2). Up to 55 % MO was degraded after 2 h. P25 and N-CND_{py}@P25 reached 30 % and 35 % MO conversions, respectively.

These results acknowledged the improved but limited enhancement provided by the CNDs derived only from pyridine. The better performance at lower pH values can be attributed to a better electrostatic accommodation of the anionic dye pollutant with the N-CNDs@P25 composites. These composites contain a greater number of N sites that can be potentially protonated at lower pH values, especially the N-CND_{py}^{NH3} and the N-CND_{py}^{ph} (see Fig. 3j-l). These conversion levels outperform other photocatalysts containing plasmonic noble metal NPs [51] and level up with other composites containing CNDs working under visible light irradiation[2], although there are also some carbon-nitride composites that reach higher conversion values [52].

In an attempt to establish the governing photo-activation mechanisms, the N-CND@P25 composites were irradiated in the presence of different fluorescent probes, selective to different ROS. Remarkably, all the N-CND@P25 hybrids exhibited a strong capability to oxidize ABDA,

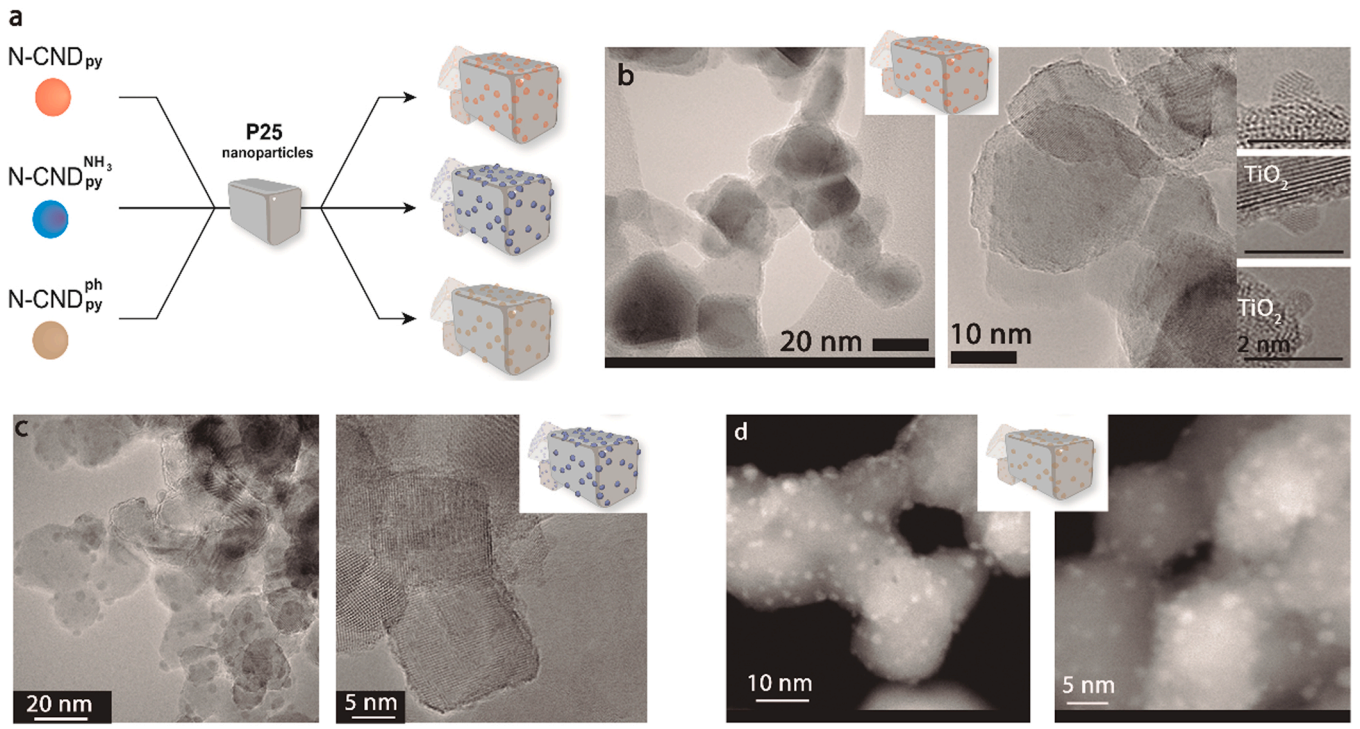

Fig. 3. Assembly of N-CNDs and P25 nanoparticles: a) Simplified scheme of the assembly mechanism; b) TEM and HRTEM images corresponding to the N-CND$_{py}$@P25 composite; c) TEM and HRTEM images corresponding to the N-CND$_{py}^{NH3}$@P25 composite; d) HAADF-STEM images corresponding to the N-CND$_{py}^{ph}$@P25 composite.

a well-known singlet oxygen trap molecule (Fig. 4h to j), even in the absence of H_2O_2 (Fig. 4k). The N-CND@P25 composites showed a strong photosensitizing capability to transfer energy from molecular $^3O_2$ into the highly active singlet oxygen $^1O_2$ since the ABDA signal was immediately quenched in all the cases due to the selective formation of an endoperoxide with non-emitting characteristics [53] (Fig. 4h to k). Moreover, we found out that O_2 was clearly necessary to obtain singlet oxygen species at short reaction rates after checking the evolution of ABDA in a suspension purged with Ar (Fig. 4g). The role of H_2O_2 seems not especially relevant to form this specific ROS, probably because evolves to other species more likely to be formed (vide infra). Still, light induced H_2O_2 disproportionation [54,55] seems like a plausible side mechanism (Fig. 4g) [56–59]. Other mechanisms to form $^1O_2$ either via oxidation of superoxide anions ($^{\bullet}O_2^-$) or via the Haber-Weiss reaction can be ruled out since these reactions typically require active metal sites to catalyze those specific pathways [60]. The capacity of CNDs to generate $^1O_2$ has been previously reported for N-enriched structures [53]. Graphene structures containing urea and thiourea also claimed this singlet oxygen production [61]. In contrast, recent studies with graphene oxide NPs have shown a very limited capacity to produce this $^1O_2$ species [62]. It is also noteworthy that P25 NPs can induce the generation of singlet oxygen as well at a slower rate than in the presence of the N-CNDs (Fig. 4e). This is probably due to the small absorption fraction of P25 in the UV-blue emitting window of the white LED. Finally, we observed a quenching of the ABDA signal during the photolysis control experiments (in the absence of photocatalysts) that has been previously reported by other authors with no specific reasons or attributed to partial bleaching [63–65].

Alternatively, the oxidation of NaTA was selected as a fluorimetric reaction to determine the formation of hydroxyl radicals ($^{\bullet}OH$) (see Experimental section for further details and Fig. 5a-b). Interestingly, the N-CND$_{py}$ and the N-CND$_{py}^{NH3}$ derived hybrids showed a stronger capacity to generate hydroxyls than the N-CND$_{py}^{Ph}$@P25 photocatalyst or the uncoated P25 NPs (Fig. 5a). This can be attributed to the lower presence of C-O functional groups in the latter according to XPS analysis (Fig. S1 and Table S1) that have been attributed as responsible for the peroxidase-mimicking response of other carbon nanodots reported in the literature [56–59]. A similar trend was observed regarding the generation of superoxide radicals in the presence of DHE [20,40] with the N-CND$_{py}^{Ph}$@P25 photocatalyst exhibiting a lower fluorescence response (Fig. 5c-d). It is indicative that these CNDs retrieved from the laser-driven pyrolysis of phtalocyanine and pyridine possess a preferential ROS generation mechanism via singlet oxygen species as expected from these type of macromolecules. It also reveals how the control of the surface functional groups (N-enriched vs. O-enriched) somehow directs the specific excitation pathways leading to different ROS.

4. Conclusions

Laser driven pyrolysis of organic precursors co-fed with either gas or solid containing N atoms appears as a promising synthesis technique to allow an exquisite control of the doping levels in carbogenic dots. The different N-doped CNDs have demonstrated a strong photosensitizing capacity under irradiation with visible light. Interestingly, we have observed that increasing the concentration of C-N surface groups at the expense of reducing the presence of C-O entities: (i) favors a major population of intermediate energy levels that lower the band gap of carbon dots thereby favoring a better hybridization with P25 levels and maximizing the absorption of LED photons; (ii) facilitates the protonation of aminated groups at lower pH values and promotes a better electrostatic attraction of the anionic dye to promote its degradation; (iii) promotes a preferential generation of singlet oxygen species over other oxidizing species such as hydroxyl or superoxide radicals. This photoactivity was demonstrated with the enhanced photodegradation of methyl orange and the generation of multiple ROS that paves the way for a wide range of potential applications beyond environmental remediation, including photodynamic therapy, selective organic chemistry or solar-driven reactions [8,10,16,34–37,24].

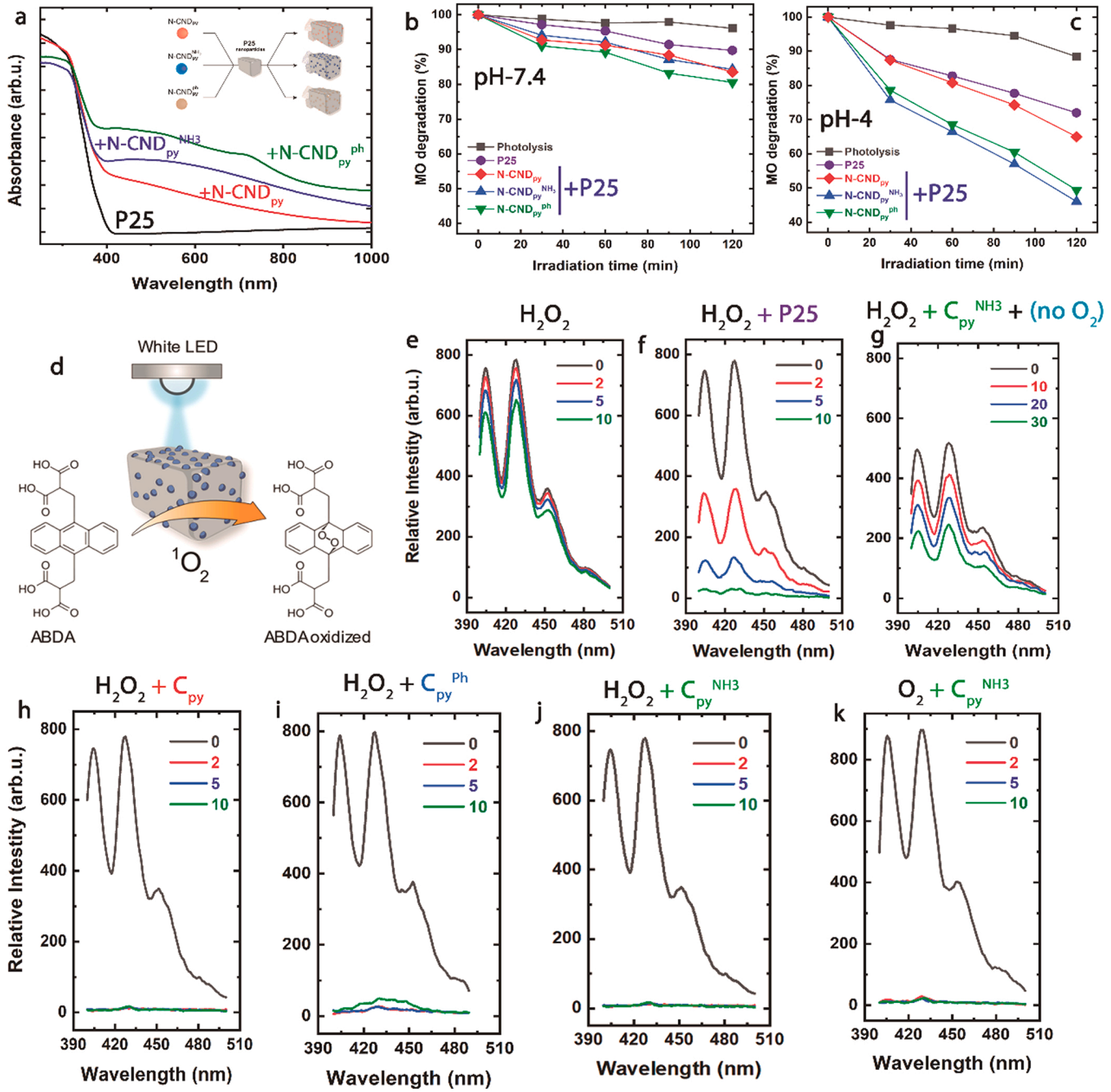

Fig. 4. Photoreactivity and singlet oxygen generation of the N-CND@P25 photocatalysts under white LED illumination: a) UV-Vis absorption spectra of the hybrids and the uncoated P25 NPs, respectively; b)-c) MO degradation percentage at different irradiation time intervals and different pH (4 and 7.4, respectively) under white LED irradiation; photolysis and uncoated P25 were also tested as references; d) Schematic display of the singlet oxygen trapping reaction occurring in the presence of ABDA; e) Evolution of ABDA in the presence of H_2O_2 and LED irradiation (photolysis in the absence of photocatalyst); f) Evolution of ABDA in the presence of H_2O_2, LED and bare P25 NPs; g) Singlet oxygen generation after removing O_2 from the aqueous media in the presence of N-CND$_{py}^{NH3}$@P25, H_2O_2 and LED irradiation; h) Singlet oxygen generation in the presence of N-CND$_{py}$@P25, H_2O_2 and LED irradiation; i) Singlet oxygen generation in the presence of N-CND$_{py}^{Py}$@P25, H_2O_2 and LED irradiation; j) Singlet oxygen generation in the presence of N-CND$_{py}^{NH3}$@P25, H_2O_2 and LED irradiation; k) Singlet oxygen generation after removing O_2 from the aqueous media in the presence of N-CND$_{py}^{NH3}$@P25 and LED irradiation (no addition of H_2O_2).

CRediT authorship contribution statement

Conceptualization: G.M., J.L.H.; Methodology: G.M.; A.M.; J.B.A.; E. C.; F.H.; J.L.H.; Validation: A.M., G.M., F.H.; Formal analysis: A.M., F.H., G.M., J.B.A., A.L., J.L.H; Investigation: A.M., J.B.A., F.H., G.M., E.C.; Data Curation: A.M., J.L.H., F.H., J.B.A.; Writing: J.L.H. with contribution of all the authors; Visualization: J.B.A., A.M., J.L.H., F.H.; Supervision: G.M., J.L.H.

Declaration of Competing Interest

The authors declare that they have no known competing financial interests or personal relationships that could have appeared to influence the work reported in this paper.

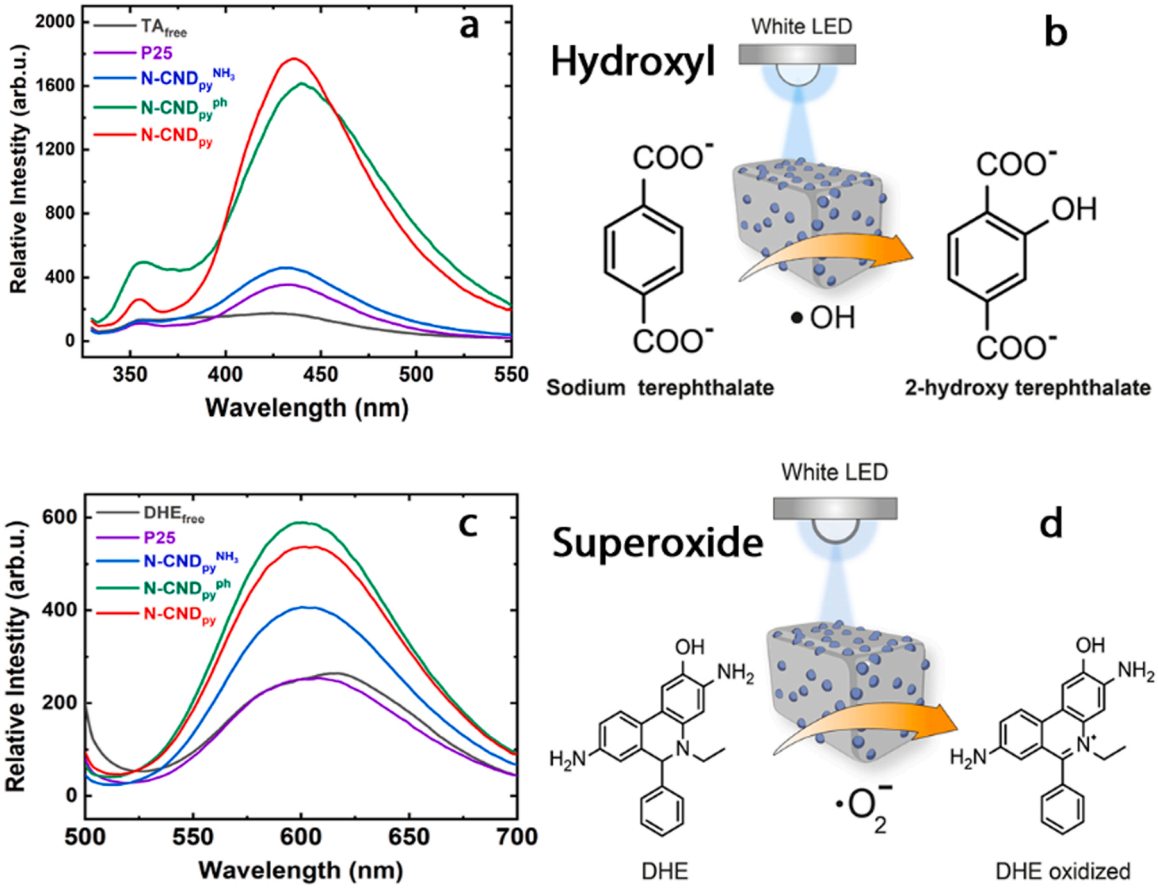

Fig. 5. Detection of additional ROS generated in the presence of different N-CND@P25 hybrids irradiated under white LED: a) Detection of hydroxyl radicals after 10 min of irradiation using disodium terephthalate (NaTA) as fluorescent probe; Photolysis experiments in the absence of photocatalyst or in the presence of uncoated P25 NPs are also included; b) Schematic display showing the specific conversion of NaTA into the fluorescent reaction product (2-hydroxy disodium terephthalate) when reacting with •OH radicals; c) Fluorescence spectra after 10 min of reaction which shows the fluorescence signal of the DHE oxidized species, indicative of the presence of superoxide radicals; d) Scheme displaying the specific reaction between superoxide anion and DHE.

Data Availability

Data will be made available on request.

Acknowledgements

Financial support from the European Research Council (ERC-Advanced Grant CADENCE number 742684), the FP7 People Program (NANOLIGHT-294094) and the Spanish Research Agency (LAERTES-PID2020-114926RB-I00) are acknowledged. The TEM measurements were conducted at the Laboratorio de Microscopias Avanzadas, ICTS ELECMI, Spain. The synthesis of materials has been performed by the Platform of Production of Biomaterials and Nanoparticles of the NANBIOSIS ICTS, more specifically by the Nanoparticle Synthesis Unit of the CIBER in BioEngineering, Biomaterials & Nanomedicine (CIBER-BBN). J.B-A. acknowledges the Spanish Government for an FPU predoctoral contract. F.H. acknowledges the Generalitat Valenciana and the European Social Fund for an APOSTD fellowship (APOSTD/2021/196). The authors thank Dr. Silvia Irusta for her help with the XPS acquisition of spectra.

Appendix A. Supporting information

Supplementary data associated with this article can be found in the online version at doi:10.1016/j.cattod.2023.114214.

References

[1] J. Yu, X. Yong, Z. Tang, B. Yang, S. Lu, Theoretical understanding of structure–property relationships in luminescence of carbon dots, J. Phys. Chem. Lett. 12 (2021) 7671–7687.
[2] K. Akbar, E. Moretti, A. Vomiero, Carbon dots for photocatalytic degradation of aqueous pollutants: recent advancements, Adv. Opt. Mater. 9 (2021), 2100532.
[3] J. Bonet-Aleta, J.I. Garcia-Peiro, J.L. Hueso, Engineered nanostructured photocatalysts for cancer therapy, Catalysts 12 (2022).
[4] N. Mas, J.L. Hueso, G. Martinez, A. Madrid, R. Mallada, M.C. Ortega-Liebana, C. Bueno-Alejo, J. Santamaria, Laser-driven direct synthesis of carbon nanodots and application as sensitizers for visible-light photocatalysis, Carbon 156 (2020) 453–462.
[5] J.I. Garcia-Peiro, J. Bonet-Aleta, C.J. Bueno-Alejo, J.L. Hueso, Recent advances in the design and photocatalytic enhanced performance of gold plasmonic nanostructures decorated with non-titania based semiconductor heterononoarchitectures, Catalysts 10 (2020).
[6] M.C. Ortega-Liebana, J.L. Hueso, S. Ferdousi, R. Arenal, S. Irusta, K.L. Yeung, J. Santamaria, Extraordinary sensitizing effect of co-doped carbon nanodots derived from mate herb: application to enhanced photocatalytic degradation of chlorinated wastewater compounds under visible light, Appl. Catal. B-Environ. 218 (2017) 68–79.
[7] M.C. Ortega-Liebana, N.X. Chung, R. Limpens, L. Gomez, J.L. Hueso, J. Santamaria, T. Gregorkiewicz, Uniform luminescent carbon nanodots prepared by rapid pyrolysis of organic precursors confined within nanoporous templating structures, Carbon 117 (2017) 437–446.
[8] G.A.M. Hutton, B.C.M. Martindale, E. Reisner, Carbon dots as photosensitisers for solar-driven catalysis, Chem. Soc. Rev. 46 (2017) 6111–6123.
[9] H.J. Liu, X.J. Wang, H. Wang, R.R. Nie, Synthesis and biomedical applications of graphitic carbon nitride quantum dots, J. Mater. Chem. B 7 (2019) 5432–5448.
[10] G.A.M. Hutton, B. Reuillard, B.C.M. Martindale, C.A. Caputo, C.W.J. Lockwood, J. N. Butt, E. Reisner, Carbon dots as versatile photosensitizers for solar-driven catalysis with redox enzymes, J. Am. Chem. Soc. 138 (2016) 16722–16730.

[11] H.J. Yu, R. Shi, Y.F. Zhao, G.I.N. Waterhouse, L.Z. Wu, C.H. Tung, T.R. Zhang, Smart utilization of carbon dots in semiconductor photocatalysis, Adv. Mater. 28 (2016) 9454–9477.
[12] F. Arcudi, L. Dordevic, M. Prato, Design, synthesis, and functionalization strategies of tailored carbon nanodots, Acc. Chem. Res. 52 (2019) 2070–2079.
[13] Y. Zhou, W. Zhang, R.M. Leblanc, Structure–property–activity relationships in carbon dots, J. Phys. Chem. B (2022).
[14] M.F. Kuehnel, E. Reisner, Solar hydrogen generation from lignocellulose, Angew. Chem. - Int. Ed. 57 (2018) 3290–3296.
[15] B.C.M. Martindale, E. Joliat, C. Bachmann, R. Alberto, E. Reisner, Clean donor oxidation enhances the H-2 evolution activity of a carbon quantum dot-molecular catalyst photosystem, Angew. Chem. -Int. Ed. 55 (2016) 9402–9406.
[16] C.M. Pichler, T. Uekert, E. Reisner, Photoreforming of biomass in metal salt hydrate solutions, Chem. Commun. 56 (2020) 5743–5746.
[17] B.C.M. Martindale, G.A.M. Hutton, C.A. Caputo, E. Reisner, Solar hydrogen production using carbon quantum dots and a molecular nickel catalyst, J. Am. Chem. Soc. 137 (2015) 6018–6025.
[18] A. Mehta, A. Mishra, S. Basu, N.P. Shetti, K.R. Reddy, T.A. Saleh, T.M. Aminabhavi, Band gap tuning and surface modification of carbon dots for sustainable environmental remediation and photocatalytic hydrogen production – a review, J. Environ. Manag. 250 (2019), 109486.
[19] M. Carmen Ortega-Liebana, J.L. Hueso, S. Ferdousi, R. Arenal, S. Irusta, K.L. Yeung, J. Santamaria, Extraordinary sensitizing effect of co-doped carbon nanodots derived from mate herb: Application to enhanced photocatalytic degradation of chlorinated wastewater compounds under visible light, Appl. Catal. B-Environ. 218 (2017) 68–79.
[20] M. Carmen Ortega-Liebana, M. Mar Encabo-Berzosa, A. Casanova, M. Desiree Pereboom, J. Octavio Alda, J.L. Hueso, J. Santamaria, Upconverting carbon nanodots from ethylenediaminetetraacetic acid (EDTA) as near-infrared activated phototheranostic agents, Chem. -A Eur. J. 25 (2019) 5539–5546.
[21] M.C. Ortega-Liebana, M.M. Encabo-Berzosa, M.J. Ruedas-Rama, J.L. Hueso, Nitrogen-induced transformation of vitamin C into multifunctional up-converting carbon nanodots in the visible-NIR range, Chem. -A Eur. J. 23 (2017) 3067–3073.
[22] M.C. Ortega-Liebana, J.L. Hueso, S. Ferdousi, K.L. Yeung, J. Santamaria, Nitrogen-doped luminescent carbon nanodots for optimal photo-generation of hydroxyl radicals and visible-light expanded photo-catalysis, Diam. Relat. Mater. 65 (2016) 176–182.
[23] C. Ji, Y. Zhou, R.M. Leblanc, Z. Peng, Recent developments of carbon dots in biosensing: a review, ACS Sens. 5 (2020) 2724–2741.
[24] A. Madrid, A. Martín-Pardillos, J. Bonet-Aleta, M. Sancho-Albero, G. Martinez, J. Calzada-Funes, P. Martin-Duque, J. Santamaria, J.L. Hueso, Nitrogen-doped carbon nanodots deposited on titania nanoparticles: Unconventional near-infrared active photocatalysts for cancer therapy, Catalysis Today 419 (2023) 114154.
[25] R.Q. Ye, Y. Chyan, J.B. Zhang, Y.L. Li, X. Han, C. Kittrell, J.M. Tour, Laser-induced graphene formation on wood, Adv. Mater. 29 (7pp) (2017), 1702211.
[26] A. Galvez, N. Herlin-Boime, C. Reynaud, C. Clinard, J.N. Rouzaud, Carbon nanoparticles from laser pyrolysis, Carbon 40 (2002) 2775–2789.
[27] I. Morjan, I. Voicu, F. Dumitrache, I. Sandu, I. Soare, R. Alexandrescu, E. Vasile, I. Pasuk, R.M.D. Brydson, H. Daniels, B. Rand, Carbon nanopowders from the continuous-wave CO_2 laser-induced pyrolysis of ethylene, Carbon 41 (2003) 2913–2921.
[28] M.T. Swihart, Vapor-phase synthesis of nanoparticles, Curr. Opin. Colloid Interface Sci. 8 (2003) 127–133.
[29] G. Martinez, A. Malumbres, A. Lopez, R. Mallada, J.L. Hueso, J. Santamaria, Laser-assisted production of carbon-encapsulated Pt-Co alloy nanoparticles for preferential oxidation of carbon monoxide, Front. Chem. 6-Art.487 (2018) 10.
[30] A. Malumbres, G. Martinez, J.L. Hueso, J. Gracia, R. Mallada, A. Ibarra, J. Santamaria, Facile production of stable silicon nanoparticles: laser chemistry coupled to in situ stabilization via room temperature hydrosilylation, Nanoscale 7 (2015) 8566–8573.
[31] A. Malumbres, G. Martinez, R. Mallada, J.L. Hueso, O. Bomati-Miguel, J. Santamaria, Continuous production of iron-based nanocrystals by laser pyrolysis. Effect of operating variables on size, composition and magnetic response, Nanotechnology 24 (2013).
[32] S.H. Wu, R.H. Zhou, H.J. Chen, J.Y. Zhang, P. Wu, Highly efficient oxygen photosensitization of carbon dots: the role of nitrogen doping, Nanoscale 12 (2020) 5543–5553.
[33] G. Martinez, A. Malumbres, R. Mallada, J.L. Hueso, S. Irusta, O. Bomati-Miguel, J. Santamaria, Use of a polyol liquid collection medium to obtain ultrasmall magnetic nanoparticles by laser pyrolysis, Nanotechnology 23 (2012).
[34] P. Di Mascio, G.R. Martinez, S. Miyamoto, G.E. Ronsein, M.H.G. Medeiros, J. Cadet, Singlet molecular oxygen reactions with nucleic acids, lipids, and proteins, Chem. Rev. 119 (2019) 2043–2086.
[35] A.A. Ghogare, A. Greer, Using singlet oxygen to synthesize natural products and drugs, Chem. Rev. 116 (2016) 9994–10034.
[36] R. Ossola, O.M. Jonsson, K. Moor, K. McNeill, Singlet oxygen quantum yields in environmental waters, Chem. Rev. 121 (2021) 4100–4146.
[37] C. Schweitzer, R. Schmidt, Physical mechanisms of generation and deactivation of singlet oxygen, Chem. Rev. 103 (2003) 1685–1757.
[38] J. Bonet-Aleta, M. Sancho-Albero, J. Calzada-Funes, S. Irusta, P. Martin-Duque, J. L. Hueso, J. Santamaria, Glutathione-triggered catalytic response of copper-iron mixed oxide nanoparticles. Leveraging tumor microenvironment conditions for chemodynamic therapy, J. Colloid Interface Sci. 617 (2022) 704–717.
[39] J. Bonet-Aleta, M. Encinas-Gimenez, E. Urriolabeitia, P. Martin-Duque, J.L. Hueso, J. Santamaria, Unveiling the interplay between homogeneous and heterogeneous catalytic mechanisms in copper-iron nanoparticles working under chemically relevant tumour conditions, Chem. Sci. 13 (2022) 8307–8320.
[40] H. Zhao, S. Kalivendi, H. Zhang, J. Joseph, K. Nithipatikom, J. Vásquez-Vivar, B. Kalyanaraman, Superoxide reacts with hydroethidine but forms a fluorescent product that is distinctly different from ethidium: potential implications in intracellular fluorescence detection of superoxide, Free Radic. Biol. Med. 34 (2003) 1359–1368.
[41] R. Shi, Z. Li, H.J. Yu, L. Shang, C. Zhou, G.I.N. Waterhouse, L.Z. Wu, T.R. Zhang, Effect of nitrogen doping level on the performance of N-doped carbon quantum Dot/TiO2 composites for photocatalytic hydrogen evolution, Chemsuschem 10 (2017) 4650–4656.
[42] S. Maldonado, S. Morin, K.J. Stevenson, Structure, composition, and chemical reactivity of carbon nanotubes by selective nitrogen doping, Carbon 44 (2006) 1429–1437.
[43] J.P. Boudou, A. Martinez-Alonzo, J.M.D. Tascon, Introduction of acidic groups at the surface of activated carbon by microwave-induced oxygen plasma at low pressure, Carbon 38 (2000) 1021–1029.
[44] A. Cuesta, P. Dhamelincourt, J. Laureyns, A. Martinez-Alonso, J.M.D. Tascon, Raman microprobe studies on carbon materials, Carbon 32 (1994) 1523–1532.
[45] J.R. Pels, F. Kapteijn, J.A. Moulijn, Q. Zhu, K.M. Thomas, Evolution of nitrogen functionalities in carbonaceous materials during pyrolysis, Carbon 33 (1995) 1641–1653.
[46] J.L. Hueso, J.P. Espinos, A. Caballero, J. Cotrino, A.R. Gonzalez-Elipe, XPS investigation of the reaction of carbon with NO, O-2, N-2 and H2O plasmas, Carbon 45 (2007) 89–96.
[47] K. Hola, M. Sudolska, S. Kalytchuk, D. Nachtigallova, A.L. Rogach, M. Otyepka, R. Zboril, Graphitic nitrogen triggers red fluorescence in carbon dots, ACS Nano 11 (2017) 12402–12410.
[48] Y. Xiong, J. Schneider, C.J. Reckmeier, H. Huang, P. Kasak, A.L. Rogach, Carbonization conditions influence the emission characteristics and the stability against photobleaching of nitrogen doped carbon dots, Nanoscale 9 (2017) 11730–11738.
[49] K.P. Gong, F. Du, Z.H. Xia, M. Durstock, L.M. Dai, Nitrogen-doped carbon nanotube arrays with high electrocatalytic activity for oxygen reduction, Science 323 (2009) 760–764.
[50] S.Y. Wang, D.S. Yu, L.M. Dai, Polyelectrolyte functionalized carbon nanotubes as efficient metal-free electrocatalysts for oxygen reduction, J. Am. Chem. Soc. 133 (2011) 5182–5185.
[51] L. Gomez, J.L. Hueso, M.C. Ortega-Liebana, J. Santamaria, S.B. Cronin, Evaluation of gold-decorated halloysite nanotubes as plasmonic photocatalysts, Catal. Commun. 56 (2014) 115–118.
[52] Q. Liu, L. Zhou, J. Gao, S. Wang, L. Liu, S. Liu, Surface chemistry-dependent activity and comparative investigation on the enhanced photocatalytic performance of graphitic carbon nitride modified with various nanocarbons, J. Colloid Interface Sci. 569 (2020) 12–21.
[53] S. Wu, R. Zhou, H. Chen, J. Zhang, P. Wu, Highly efficient oxygen photosensitization of carbon dots: the role of nitrogen doping, Nanoscale 12 (2020) 5543–5553.
[54] H. Ikai, K. Nakamura, M. Shirato, T. Kanno, A. Iwasawa, K. Sasaki, Y. Niwano, M. Kohno, Photolysis of hydrogen peroxide, an effective disinfection system via hydroxyl radical formation, Antimicrob. Agents Chemother. 54 (2010) 5086–5091.
[55] E. Kalay, H. Kilic, M. Catir, M. Cakici, C. Kazaz, Generation of singlet oxygen (O-1 (2)) from hydrogen peroxide decomposition by in situ generated hypervalent iodoarene reagents, Pure Appl. Chem. 86 (2014) 945–952.
[56] J.Y. Zhang, X.M. Lu, D.D. Tang, S.H. Wu, X.D. Hou, J.W. Liu, P. Wu, Phosphorescent carbon dots for highly efficient oxygen photosensitization and as photo-oxidative nanozymes, Acs Appl. Mater. Interfaces 10 (2018) 40808–40814.
[57] J. Saleem, L.M. Wang, C.Y. Chen, Carbon-based nanomaterials for cancer therapy via targeting tumor microenvironment, Adv. Healthc. Mater. 7 (2018).
[58] M. Shamsipur, A. Barati, S. Karami, Long-wavelength, multicolor, and white-light emitting carbon-based dots: achievements made, challenges remaining, and applications, Carbon 124 (2017) 429–472.
[59] D. Lu, R. Tao, Z. Wang, Carbon-based materials for photodynamic therapy: a mini-review, Front. Chem. Sci. Eng. 13 (2019) 310–323.
[60] Q.Y. Yi, J.H. Ji, B. Shen, C.C. Dong, J. Liu, J.L. Zhang, M.Y. Xing, Singlet oxygen triggered by superoxide radicals in a molybdenum cocatalytic fenton reaction with enhanced redox activity in the environment, Environ. Sci. Technol. 53 (2019) 9725–9733.
[61] S.P. Jovanovic, Z. Syrgiannis, M.D. Budimir, D.D. Milivojevic, D.J. Jovanovic, V. B. Pavlovic, J.M. Papan, M. Bartenwerfer, M.M. Mojsin, M.J. Stevanovic, B.M. T. Markovic, Graphene quantum dots as singlet oxygen producer or radical quencher the matter of functionalization with urea/thiourea, Mater. Sci. Eng. C. -Mater. Biol. Appl. 109 (2020).
[62] C. Felip-Leon, M. Puche, J.F. Miravet, F. Galindo, M. Feliz, A spectroscopic study to assess the photogeneration of singlet oxygen by graphene oxide, Mater. Lett. 251 (2019) 45–51.
[63] Y. Yu, J. Geng, E.Y.X. Ong, V. Chellappan, Y.N. Tan, Bovine serum albulmin protein-templated silver nanocluster (BSA-Ag13): an effective singlet oxygen generator for photodynamic cancer therapy, Adv. Healthc. Mater. 5 (2016) 2528–2535.
[64] W. Zhu, Y. Li, S. Guo, W.-J. Guo, T. Peng, H. Li, B. Liu, H.-Q. Peng, B.Z. Tang, Stereoisomeric engineering of aggregation-induced emission photosensitizers towards fungal killing, Nat. Commun. 13 (2022) 7046.
[65] S. Xu, Y. Yuan, X. Cai, C.-J. Zhang, F. Hu, J. Liang, G. Zhang, D. Zhang, B. Liu, Tuning the singlet-triplet energy gap: a unique approach to efficient

photosensitizers with aggregation-induced emission (AIE) characteristics, Chem. Sci. 6 (2015) 5824–5830.